International Journal of Nanomedicine

Dovepress

open access to scientific and medical research

Open Access Full Text Article

ORIGINAL RESEARCH

Hollow Prussian Blue Nanospheres for Photothermal/Chemo-Synergistic Therapy

This article was published in the following Dove Press journal:
International Journal of Nanomedicine

Long Lu[1]
Chuanbin Zhang[1]
Bingfang Zou[1,2]
Yongqiang Wang[1]

[1]Key Laboratory for Special Functional Materials of the Ministry of Education, Henan University, Kaifeng 475004, People's Republic of China; [2]School of Physics and Electronics, Henan University, Kaifeng 475004, People's Republic of China

Background: The integration of NIR photothermal therapy and chemotherapy is considered as a promising technique for future cancer therapy. Hollow Prussian nanospheres have attracted much attention due to excellent near-infrared photothermal conversion effect and drug-loading capability within an empty cavity. However, to date, the hollow Prussian nanospheres have been prepared by a complex procedure or in organic media, and their shell thickness and size cannot be controlled. Thus, a simple and controllable route is highly desirable to synthesize hollow Prussian nanospheres with controllable parameters.

Materials and Methods: Here, in our designed synthesis route, the traditional $FeCl_3$ precursor was replaced with Fe_2O_3 nanospheres, and then the Prussian blue (PB) nanoparticles were engineered into hollow-structured PB (HPB) nanospheres through an interface reaction, where the Fe_2O_3 colloidal template provides Fe^{3+} ions. The reaction mechanism and control factors of HPB nanospheres were systematically investigated. Both in vitro and in vivo biological effects of the as-synthesized HPB nanospheres were evaluated in detail.

Results: Through systematical experiments, a solvent-mediated interface reaction mechanism was put forward, and the parameters of HPB nanospheres could be easily adjusted by growth time and template size under optimal water and ethanol ratio. The in vitro tests show the rapid and remarkable photothermal effects of the as-prepared HPB nanospheres under NIR laser irradiation (808 nm). Meanwhile, HPB nanospheres also demonstrated a high DOX loading capacity of 440 mg g^{-1} as a drug carrier, and the release of the drug can be regulated by the heat from PB shell under the exposure of an NIR laser. The in vivo experiments confirmed the outstanding performance of HPB nanospheres in photothermal/chemo-synergistic therapy of cancer.

Conclusion: A solvent-mediated template route was developed to synthesize hollow Prussian blue (HPB) nanospheres in a simple and controllable way. The in vitro and in vivo results demonstrate the as-synthesized HPB nanospheres as a promising candidate due to their low toxicity and high efficiency for cancer therapy.

Keywords: template, Prussian blue, hollow nanospheres, chemotherapy, photothermal therapy

Introduction

The most traditional cancer therapies include chemotherapy, radiotherapy, and surgery, where the patients may suffer from serious side effects and unsatisfactory treatment outcomes. With the advancement of nanomaterials and nanotechnology, various nanomaterials were fabricated into hollow or porous structures to load and deliver drugs, therapeutic radioisotopes, and other therapeutic agents into targeted sites.[1–3] Lots of researchers reported that the nanocarrier drug delivery systems demonstrated unparalleled advantages compared with pristine therapeutic agents.

Correspondence: Yongqiang Wang
Email wangyq@henu.edu.cn

submit your manuscript | www.dovepress.com
DovePress
http://doi.org/10.2147/IJN.S252505

For example, nanocarriers show high loading capacity and sufficient protection from harsh surroundings, avoiding unnecessary drug loss and side effects. Moreover, the efficiency of many conventional pharmaceutical therapies can be significantly improved with the aid of drug delivery systems.[4,5]

Meanwhile, other new treatments have also been developed to treat cancer, including photothermal therapy, photodynamic therapy, gene therapy, and immunotherapy, which can potentially improve the therapeutic outcomes.[6,7] Among them, photothermal therapy (PTT) can trigger the death of cancer cells by converting light energy into heat.[8] PTT offers certain advantages including precise targeting of tumors with adjustable irradiation dosage and non-invasive treatment, which have attracted much attention in the field of biology during the last few years.[9] A number of photothermal nanoagents, such as gold with various nanostructures, carbon nanomaterials, copper-based nanocrystals, sulfide nanosheets, and metal oxide nanoparticles have been reported to show photothermal effects to kill cancer cells.[10]

Recently, to further improve the therapeutic effect, several different therapies were combined for synergistic cancer treatment.[11] For example, photothermal agents alone are not enough due to the unavoidable depth-dependent attenuation of laser intensity. The integration of photothermal ablation and chemotherapy in one system has become a hot research field. The key point of chemo-thermal therapy is the design and synthesis of photothermal agents with high-efficiency photothermal effects and high drug-loading capacity.[12–15]

Prussian blue (PB) nanomaterials have excellent near-infrared photothermal conversion effect, and have great potential as a new generation of photothermal agents to replace traditional photothermal agents.[16] A large number of studies have shown that Prussian blue nanoparticles have some important characteristics in the biological environment, such as stability in human serum and efficient cell uptake.[17–22] More importantly, PB nanoparticles are a typical US FDA-approved drug in the clinic for treatment of radioactive exposure, demonstrating absolutely approved biosafety in the human body based on sufficient clinical trials. Hollow Prussian nanoparticles have attracted much attention due to their potential to encapsulate large quantities of guest molecules within their empty core domain.[23–30] The polymer capsules with a Prussian blue analog inner shell was reported as nanocontainers to encapsulate and release a model compound; however, organic solvents were used during the emulsion-induced assembly.[31,32] Recently, hollow Prussian blue nanocubes were fabricated utilizing a self-etching reaction in the presence of PVP, but the parameters of the hollow spheres, such as size and shell thickness, were hardly controlled.[33] Moreover, it is difficult to achieve large-scale production of hollow PB nanoparticles via the above-mentioned synthetic strategies.

The template method is preferentially used to produce hollow spheres with controlled parameters, especially when the template itself is involved as a precursor in the formation of the shell (i.e. as a chemical template), and then the synthesis procedure will be simplified into an interface reaction.[34–36] It is well known that PB solid nanoparticles can be readily synthesized in water at room temperature using $FeCl_3$ and $K_4[Fe(CN)_6]$.[16] In this paper, we propose to replace $FeCl_3$ with Fe_2O_3 nanospheres to provide Fe^{3+} ions in our designed synthesis route (Scheme 1). Under optimized acidic solution, the Fe^{3+} ions released from Fe_2O_3 nanospheres would react with $[Fe(CN)_6]^{4-}$ and generate a PB shell in situ around the interface; thus, hollow PB (HPB) nanospheres could be easily obtained after Fe_2O_3 nanospheres were removed. Due to the porous shell and hollow cavity, the HPB nanospheres are suitable for the loading of doxorubicin hydrochloride (DOX). Meanwhile, the local heat from the PB shell under the exposure of NIR laser can simultaneously regulate the release of DOX, thus leading to cancer cell apoptosis in a synergistic way.

Experimental Section

Preparation of Hollow Prussian Blue (HPB) Nanospheres

The monodisperse Fe_2O_3 nanospheres were prepared through the hydrothermal reaction reported previously.[40] The as-obtained Fe_2O_3 nanospheres (15 mg) were dispersed in a water-ethanol mixture (40 mL) including PVP (0.2 g) under an ultrasound instrument for 2 h at room temperature (25°C) and mechanical stirring (300 r/min) at the same time. After 0.1 mL $K_4[Fe(CN)_6]\cdot 3H_2O$ (0.1 M) solution were added, 5 mL HCl solution (7.2 M) were introduced by a peristaltic pump. After 4 h, the product was collected by centrifugation at 8000 rpm for 5 min and washed thoroughly with deionized water and ethanol. After the product was etched with HCl solution (8 M, 5 mL) for 8 h at room temperature (25°C), hollow Prussian blue nanospheres were obtained.

Drug Loading

After 5 mg HPB nanospheres were added into 5 mL DOX solution (1 mg mL^{-1}), the mixture was kept in a shaker (SK-O180-Pro) for 24 h at room temperature. The DOX-

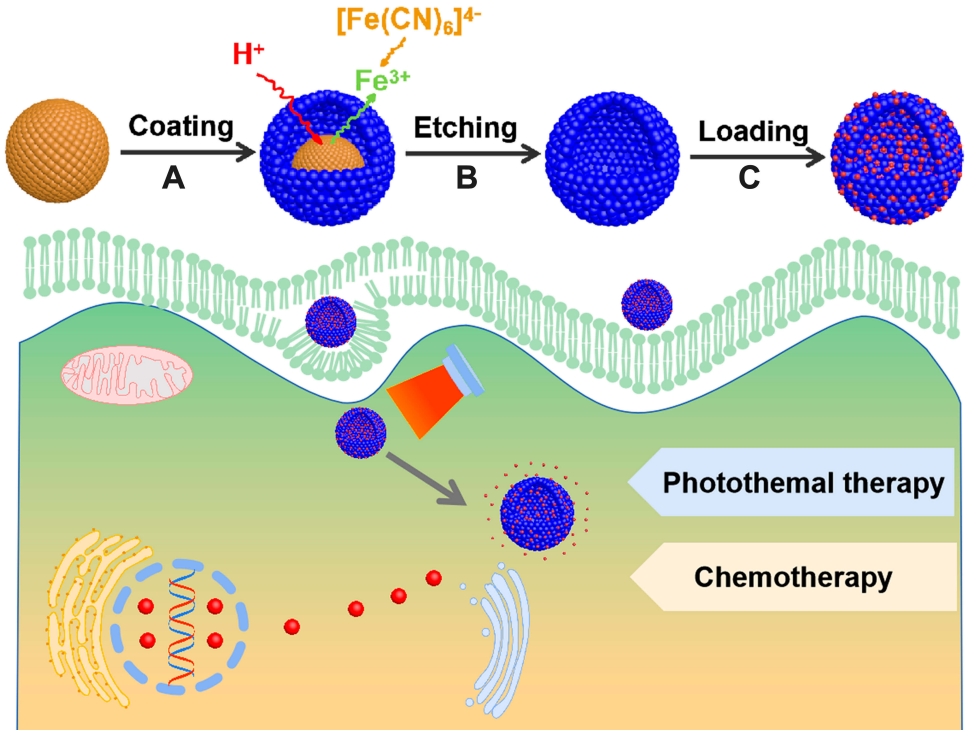

Scheme 1 The synthesis illustration of HPB nanospheres as therapy agents for photothermal/chemo-synergistic therapy of cancer.

loaded HPB nanospheres were collected by repeated centrifugation and washed three times with deionized water, and then they were dried at room temperature. The concentration of unbounded DOX was measured by UV-Vis-NIR spectroscopy with absorption intensity at 480 nm. DOX drug-loading capacity was measured using the following equation:

$$\text{Loading capacity} = (\text{total DOX} - \text{unbounded DOX}) / \text{total HPB nanospheres}$$

In vitro Drug Release of DOX

The HPB-DOX (2 mg) was packaged into a dialysis bag (MWCO = 8 kDa), and then immersed within 25 mL PBS solution at different pH (pH = 7.4 or 5.0) and temperature (37°C or 43°C) in a tube with gentle shaking. The 5 mL release solution was removed at predetermined time intervals and then an equal amount of fresh PBS was added at the same time to maintain the total solution volume constant. The release solutions were analyzed by UV-Vis-NIR spectroscopy to determine the amount of DOX released. The cumulative DOX release ratio was calculated according to the following formula:

$$\begin{cases} E_r = \frac{V_0 C_i}{m_{drug}} \times 100\% (\mathrm{i} = 1) \\ E_r = \frac{V_e \sum_1^{i-1} C_{i-1} + V_0 C_i}{m_{drug}} \times 100\% (\mathrm{i} \geq 2) \end{cases}$$

where E_r is the cumulative released ratio of DOX (%), V_e and V_0 are the volumes of the exchanged medium and the total medium, respectively (in mL), C_i is the DOX concentration of the release medium taken at the i-th time (in mg mL^{-1}), and m_{drug} is the total mass of DOX in the nanoparticles (in mg).

Photothermal Performance in vitro

The photothermal performance of the synthesized HPB nanospheres was evaluated with an infrared thermal camera. Typically, the solution of the sample was diluted to a series of concentrations of deionized water (0, 10, 25, 50, 100, and 200 μg mL^{-1}). Then, illuminated by a beam of an 808 nm laser at a power density of 1 W cm^{-2} for 5 min and the initial room temperature was 25°C. The running temperature of the solution was recorded by an infrared thermal camera every 30 s and a photo was taken at the same time.

In order to further assess the photothermal stability of the material, five cycles of NIR laser radiation were performed. Briefly, the solution of the sample with a concentration of

200 μg mL^{-1} was illuminated by an 808 nm laser at a power density of 1 W cm^{-2} for 5 min, and then the light source was turned off for another 5 min. This process was repeated 5 times to estimate the photothermal stability of HPB nanospheres.

In vitro Cytotoxicity of HPB Nanospheres

The cytotoxicity of the as-synthesized nanoparticles was evaluated with MTT assay. Typically, human cervical carcinoma cells (HeLa), purchased from Shanghai Institutes for Biological Sciences Cell Resource Center, were cultured in standard cell media cells seeded into 96-well plates and were incubated in 5% CO_2 at 37°C for 24 h. Then, different concentrations of HPB nanospheres were added into the 96-well plates and continued to be cultured for 24 h. After that, cell viability was determined using the MTT reduction assay.

In vitro Synergistic Chemo-Thermal Therapy

HeLa cells were seeded into 96-well plates at a density of 10^4 cells per well and incubated in 5% CO_2 at 37°C for 24 h. The culture medium was changed and cells were incubated with complete medium containing PBS (control), HPB nanospheres, NIR, free DOX (20 μg mL^{-1}), HPB-DOX, HPB+NIR, and HPB-DOX+NIR. The groups of HPB nanospheres and HPB-DOX have an equivalent HPB nanosphere dosage (50 μg mL^{-1}). After 4 h of incubation, excess unbound materials were removed by rinsing three times with PBS. Fresh complete medium was then added to the wells. The cells of the groups, HPB nanospheres, HPB-DOX, were exposed to 808 nm laser at a power density of 1 W cm^{-2} for 5 min for photothermal and chemo-thermal therapy treatment. Then, they were incubated again in 5% CO_2 at 37°C for 24 h. Relative cell viabilities were determined by the standard MTT assay.

Cell Uptake Assay

HeLa cells were inoculated into a confocal Petri dish at an initial cell density of 10^4 cells cm^{-2}. When the cell confluence reached around 70–80%, the culture medium was replaced with fresh media containing HPB-DOX (100 μg mL^{-1}). After culture in 5% CO_2 at 37°C for 4 h, HeLa cells were irradiated by 808 nm laser at a power density of 1 W cm^{-2} for 5 min and incubated for another 24 h. The culture medium was removed by rinsing three times with PBS. Cells were stained with Hoechst for 30 min, and rinsed three times with PBS. The cells were observed by laser scanning confocal microscope.

In vivo Infrared Thermal Imaging

All animal experiments were performed according to protocols permitted by the Animal Care Committee of Henan University. Female nude mice (4 weeks old) were purchased from Beijing Vital River Experimental Animal Technology Co., Ltd. To obtain tumor-bearing animals, HeLa cells (1×10^6) were suspended in 100 mL PBS and subcutaneously injected into the thigh of every nude mouse. The tumor-bearing mice were randomly divided into three groups (n = 3 mice per group) which were then were intratumorally injected with PBS, HPB, and DOX-HPB (10 mg kg^{-1}), respectively. The temperature of the tumor site in mice was recorded by infrared thermal imaging camera under the 808 nm laser irradiation.

In vivo Synergistic Chemo-Thermal Therapy

To investigate the therapeutic effect of chemo-thermal therapy. The tumor-bearing nude mice were randomly divided into six groups (n = 3 mice per group): (1) control group (PBS+NIR), (2) HPB group, (3) free DOX group, (4) DOX-HPB group, (5) HPB+NIR group, (6) DOX-HPB+NIR group. When the volume of tumor reached about 250–300 mm^3, the nude mice in the treatment groups were injected with PBS (200 μL), free DOX (200 μL, C_{DOX} = 2 mg mL^{-1}), HPB (200 μL, C_{HPB} = 2 mg mL^{-1}), and DOX-HPB (200 μL, C_{HPB} = 2 mg mL^{-1}) by intratumoral injection, respectively. After one day, the tumor-bearing mice of groups (1), (5) and (6) were treated with 808 nm laser (1 W cm^{-2}) for 5 min. The tumor dimensions were measured with a caliper, and the tumor volume was calculated according to the equation: Volume = (Tumor length) × (Tumor width)^2/2.

Characterization

SEM (Nova-Nano SEM 450, FEI, America) and TEM (JEOL JEM-2010, JEOL, Japan) were used to characterize the morphology. The compositions of products were analyzed by X-ray diffraction (D8-ADVANCE, Bruker, Germany) and an Infrared Fourier Transform Spectrometer (VERTEX 70, Bruker, Germany). Nitrogen adsorption isotherms were obtained at 273 K with a Quadrasorb TM SI Four Station Surface Area Analyzer and Pore Size Analyzer (Quadrasorb

SI-4, Quantachrome, America). The UV-Vis-NIR absorbance spectra of samples were obtained using a UV-Vis-NIR spectrophotometer (PE Lambda 950, PerkinElmer, America). The fluorescence image of the cells was detected by laser scanning confocal microscopy (Zeiss 880, Carl Zeiss, Germany). The average size distribution and zeta potential of the nanoparticles were assessed by the Zetasizer Nano ZS instrument (Malvern Instruments, UK).

Statistical Analysis

All experiments and measurements were carried out three times, and all results were reported as mean ± standard deviation (SD). Statistical analyses were performed using Student's *t*–test. The differences were considered statistically significant for p values <0.05.

Results and Discussion

The Design and Synthesis of HPB Nanospheres

The monodisperse Fe_2O_3 nanospheres with a diameter of 110 nm were used as a template in the present experiment in Figure 1A. Here, diluted HCl solution was added into the reaction solution to trigger the release of Fe^{3+} ions through the dissolution of the Fe_2O_3 nanospheres. According to the designed route, PB could be generated around Fe_2O_3 nanospheres through the interfacial reaction between the $[Fe(CN)_6]^{4-}$ and the released Fe^{3+} ions. As shown in Figure 1B, lots of PB nanoparticles were generated, but loosely attached around Fe_2O_3 nanospheres. Obviously, the PB nanoparticles did not form a complete shell through just simple replacement of the iron source. We noticed that the color of the supernatant was blue, which implied that lots of PB nanoparticles are generated through self-nucleation in the solution phase. It was primarily proposed that the release of Fe^{3+} ions from the Fe_2O_3 nanospheres in acidic solution was too fast, which caused the reaction to proceed mainly in the solution phase; thus, the release rate of Fe^{3+} ions from Fe_2O_3 nanospheres should be slowed down. And then ethanol was tentatively introduced into the solution to suppress the ionization of HCl, and then decrease the dissolution rate of Fe_2O_3 nanospheres. As shown in Figure 1C and D,

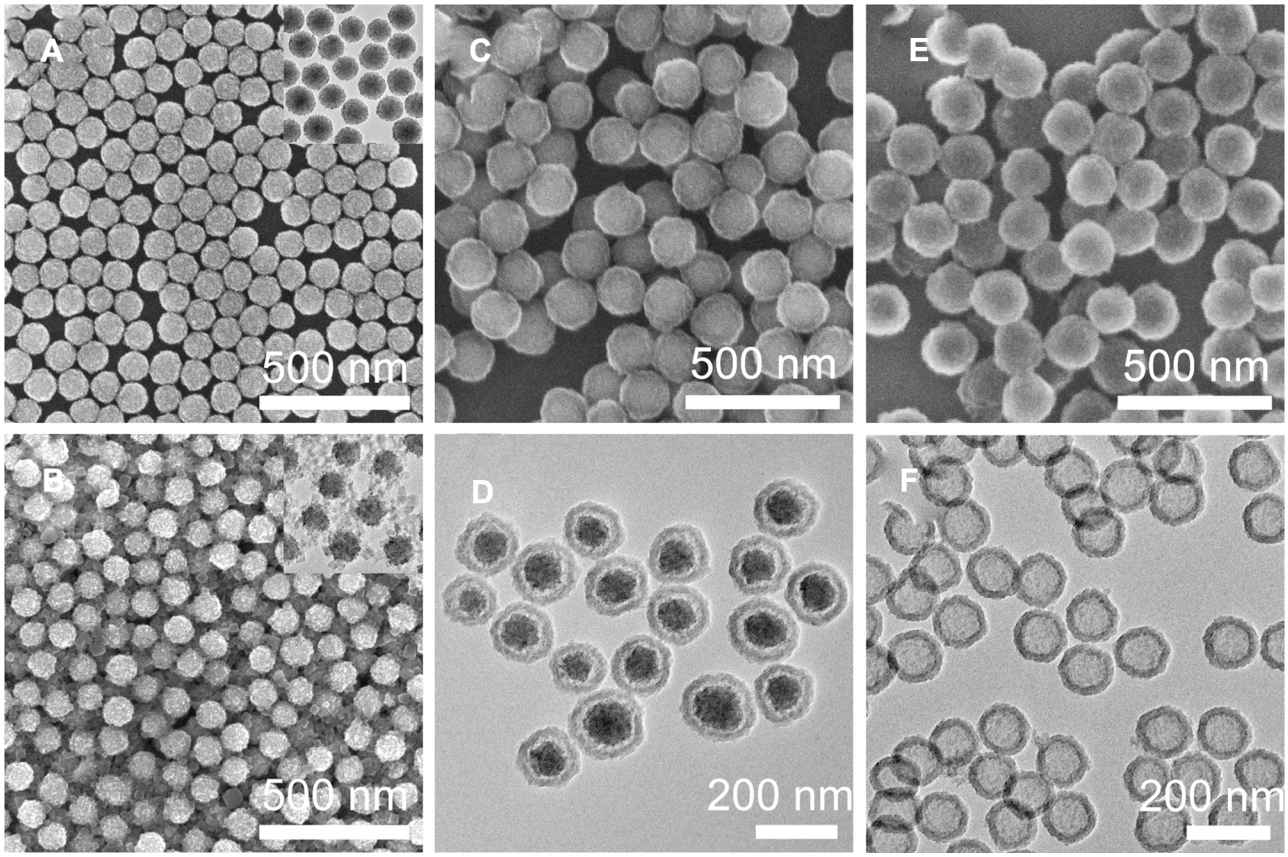

Figure 1 SEM images of the typical Fe_2O_3 nanospheres (**A**), the typical Fe_2O_3@PB composite nanospheres synthesized in pure water (**B**) and ethanol/water mixture (**C**), TEM image of the typical Fe_2O_3@PB composite nanospheres (**D**), SEM image (**E**) and TEM image (**F**) of the typical HPB nanospheres.

complete and smooth PB shells were generated with partial Fe_2O_3 colloidal template undissolved when proper ethanol was used. The PB shell copied the shape of Fe_2O_3 nanospheres perfectly and showed similar monodispersity. To create an interior hollow cavity, the residual Fe_2O_3 colloidal template was removed by treating them in 3 M HCl solution at room temperature for 8 h, and monodisperse HPB nanospheres with uniform shell (25 nm) were then obtained as seen from Figure 1E and F. From the XRD patterns of Fe_2O_3, Fe_2O_3@PB and hollow PB nanospheres (Figure S1), the diffraction peaks of PB from Fe_2O_3@PB and hollow PB nanospheres remained unchanged after acidic etching, which showed exactly the same diffraction patterns (Fm3m) assigned according to the PB crystals (JCPDS card 73–0687).[37] Furthermore, the generation of PB materials was also confirmed from their corresponding IR spectra (Figure S2), where the strong absorption peaks at 2081 cm^{-1} are characteristic CN stretching absorption bands, and the absorption bands at around 503 cm^{-1} are due to the structure of the Fe^{II}-CN-Fe^{III} linkage.[38] The above-characterized results prove the feasibility of our designed route to synthesize HPB nanospheres.

Investigating the Reaction Mechanism for Controlled Synthesis

From the above experimental results, the ethanol was found to play a critical role in the formation of the PB shell. Here the ethanol/water ratio in the solvent was precisely adjusted to investigate the effect of ethanol on the formation of PB shell. As shown in Figure 2, the HPB synthesized with different ethanol/water ratios (E/W) were sampled and characterized. When a small amount of ethanol was added with E/W = 1:8, the product in Figure 2A showed that many more PB nanoparticles were attached to Fe_2O_3 nanospheres than that synthesized in pure water in Figure 1B, indicating that the reaction site is closer to the template interface. When the content of ethanol in solution increased with E/W = 5:4, PB nanoparticles form a complete but rough shell around the residual Fe_2O_3 nanospheres in Figure 2B. With the E/W increasing to 7:2, complete PB shells with uniform shell thickness and smooth surface were generated during the reaction deposited around the Fe_2O_3 colloidal template in Figure 2C. However, when more ethanol was added (E/W = 8:1), although the Fe_2O_3 colloidal template was partially etched as seen from their reducing size, no PB shell is observed in Figure 2D, which was also proved from the IR characterizations in Figure S3. The control experiments indicated the morphology of the PB shell was indeed strongly influenced by E/W ratios, and a perfect PB shell could be realized with the optimal E/W ratio of around 7:2.

The ionization of HCl was suppressed when ethanol was introduced, which led to the slow release of Fe^{3+} ions from the Fe_2O_3 colloidal template. In such a condition, once the released Fe^{3+} ions encountered $[Fe(CN)_6]^{4-}$ ions, PB nanoparticles were intermediately deposited in situ around the template, and thus few Fe^{3+} ions could diffuse into solution phase. However, it was noticed that the Fe_2O_3 nanospheres were still dissolved to provide Fe^{3+} ions with more ethanol, which can be seen from the etched surface in Figure 2D, but PB nanoparticles were hardly detected around the residual Fe_2O_3 template. In such a condition, it could be ascribed to the low concentration of $[Fe(CN)_6]^{4-}$ nearby the Fe_2O_3 template. This result further revealed that the ionization of $K_4[Fe(CN)_6]$ was also suppressed, even more seriously than that of HCl. As a matter of fact, $K_4[Fe(CN)_6]$ was insoluble in pure ethanol. Thus, the reaction mechanism for the generation of PB shell was that both the release of Fe^{3+} from the Fe_2O_3 nanospheres and $[Fe(CN)_6]^{4-}$ from $K_4[Fe(CN)_6]$ were suppressed but matched very well under the optimal condition for the formation of the PB shell. In addition, the E/W mixed solvent also played the role of "buffer solution," where the H^+ and $[Fe(CN)_6]^{4-}$ ions would be supplied continuously through ionization balance after they were gradually consumed. Thus, the successful synthesis of HPB nanospheres was closely related to the solvent, which could efficiently mediate the deposition of PB shell around the Fe_2O_3 colloidal template.

The growth procedure of PB shell in the solvent with an optimized E/W ratio was further investigated. As shown in Figure S4a, a thin but uniform PB shell (about 10 nm) was generated around Fe_2O_3 colloidal template after 1 h, indicating that the reaction proceeded smoothly at the template interface with optimal reaction parameters. The shell became thicker (about 25 nm) gradually with reaction time in Figure S4b and c. The growth process also proved the advantage of the optimal solvent ratio, which made the reaction smoother; meanwhile, the shell with different thicknesses could be easily controlled by reaction time. In addition, the void size of HPB nanospheres determined by the template size could be adjusted by using Fe_2O_3 colloidal template with different sizes, which is another feature of the template method beside the inherited monodispersity. The HPB nanospheres with different void sizes

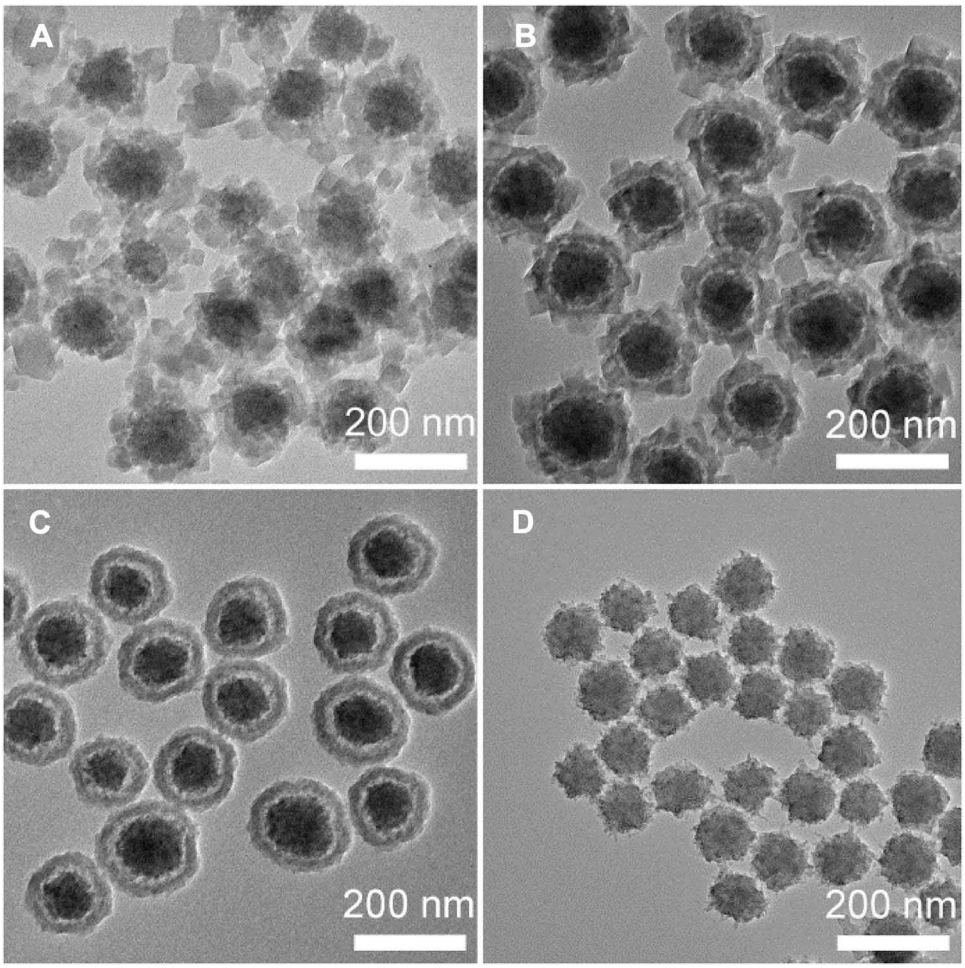

Figure 2 The TEM images of Fe_2O_3@PB composite nanospheres synthesized in solvent with different ethanol/water ratios: (**A**) 1:8, (**B**) 5:4, (**C**) 7:2, (**D**) 8:1.

could be adjusted by the template size. For example, HPB nanospheres with different void sizes of about 110, 150, and 180 nm were synthesized as shown in Figure S4d–f. The as-prepared HPB nanospheres have controllable shell thickness and hole size, which proves the superiority of the designed route, and can provide HPB nanospheres for different applications.

The Photothermal Performance of HPB Nanospheres

The UV-Vis-NIR spectrum of the as-obtained HPB nanospheres shows that they have strong absorption of NIR light (600 to 900 nm), which is in accordance with the NIR absorption of PB nanoparticles in Figure S5, where their molar absorbance is similar.[16,21] Thus, an 808 nm NIR laser was chosen in this work as the light source to investigate the photothermal conversion performance. The HPB nanosphere aqueous solutions with different concentrations (0, 10, 25, 50, 100, and 200 μg mL^{-1}) were exposed to the 808 nm laser at a power density of 1 W cm^{-2}, respectively, where the initial temperature was maintained at 25°C. As seen from Figure 3A, the temperature change (black curve) in pure water is almost negligible. However, the temperature rises quickly with their increasing content as seen in Figure 3A and B, which was obviously attributed to the photothermal effect of HPB nanospheres. For example, when 3 mL solution containing HPB nanospheres with a concentration of 100 μg mL^{-1} was irradiated for 5 min, the temperature of the solution exhibited a quick temperature increase from 25°C to 72.3°C as seen in Figure 3A. Moreover, the photothermal performance can remain without any loss after five cycles in Figure 3C, revealing the great photostability of HPB nanospheres. Unlike some other photothermal agents, such as Au nanomaterials, which would "melt" and lose their NIR absorbance after a long period of NIR laser irradiation, here HPB nanospheres are kept unchanged before and after five cycles of irradiation of NIR light (Figure 3D, inset TEM

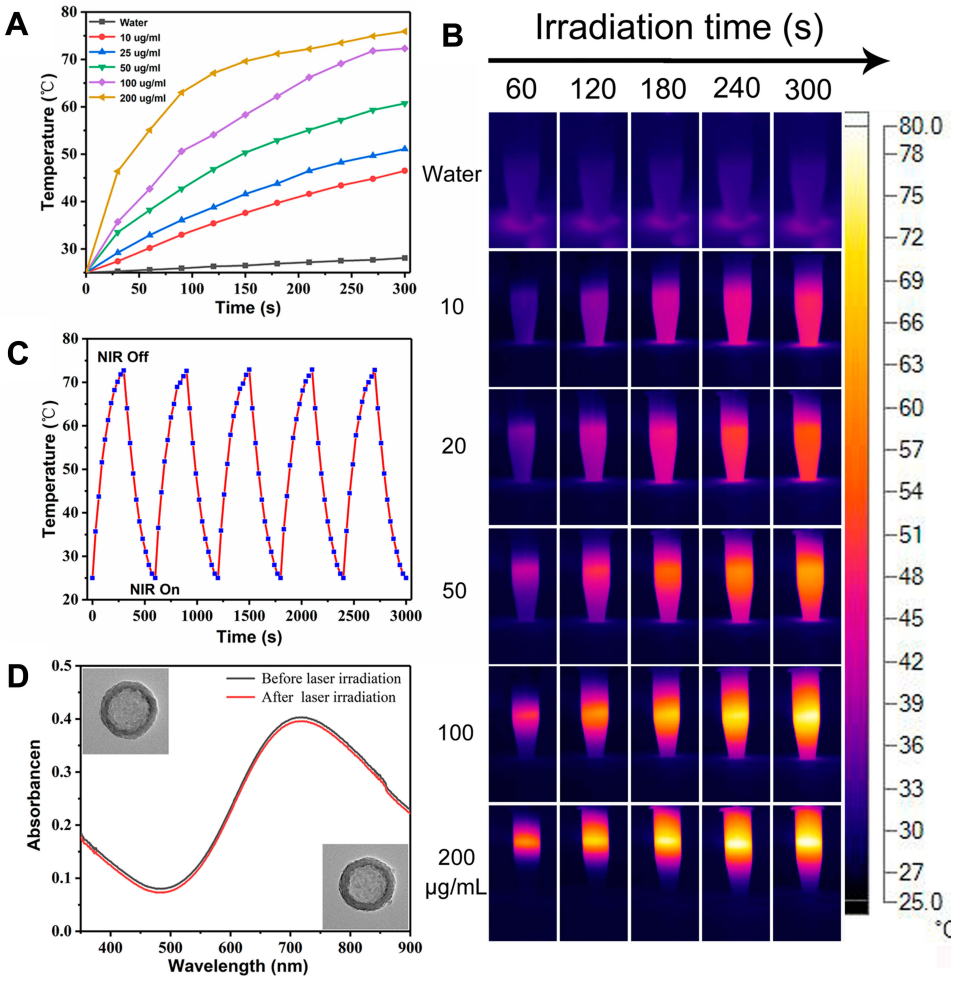

Figure 3 The photothermal property of HPB nanospheres, (**A**) heating curves of water and HPB nanospheres solutions (3 mL) with different concentrations (0, 10, 25, 50, 100, 200 μg mL^{-1}) under 808 nm laser, (**B**) corresponding infrared thermal graphs, (**C**) temperature variations of HPB nanospheres, (**D**) comparison of absorption spectra and TEM images (Inset) of Prussian blue hollow microspheres before and after irradiation.

images), and the adsorption spectra changed little; thus, all these indicated that the as-obtained HPB nanospheres can be used as ideal photothermal agents in cancer therapy.

The Loading and Release Behavior of DOX in HPB Nanospheres

The mesoporous features of HPB nanospheres were characterized through the N_2 adsorption/desorption isotherms as shown in Figure S6, and the BET specific surface area could reach about 302.9 m^2 g^{-1} with the pores peaking at 3.8 nm. Owing to hollow mesoporous structure and large specific surface area, the as-obtained HPB nanospheres can be employed as ideal carriers to encapsulate anticancer drugs.[39] As shown in Figure S7, HPB nanospheres were highly dispersible and stable in both water and blood serum with no observable aggregation within one week, which shows similar dynamic light scattering distributions. Doxorubicin (DOX) is a well-known small molecular drug for its wide clinical application in cancer therapy. Herein, DOX is chosen as a drug model and loaded into the cavity of HPB nanospheres by a common diffusion and permeation method based on their porous shell. As indicated by the UV-Vis-NIR spectroscopy and the inset digital photos of DOX solutions before and after interaction with HPB nanospheres (Figure 4A), a large amount of DOX could be loaded in HPB nanospheres. The results of the FTIR spectra of DOX, HPB nanospheres, and DOX-loaded HPB nanospheres proved the successful drug loading in Figure 4B. The loading capacity of DOX can reach 440 mg g^{-1}, and the extremely high loading capacity can be attributed to the high specific surface area of the hollow mesoporous structure, where the positively charged DOX could be bound to the negatively charged HPB nanospheres (−20.6 mV)

through electrostatic interaction, as well as strong coordinative bonding between inherent Fe(III) in the structure of HPB nanospheres and chemical groups (e.g. amino and carbonyl) of DOX.[27] Moreover, the DOX released from HPB nanospheres exhibits typical sustained pH and temperature-responsive release profiles (Figure 4C). The cumulative release of DOX from HPB nanospheres dispersed in the PBS solution in 48 h at different pH values (pH = 7.4 or 5.0) and temperatures (37°C or 43°C) is studied. It is worth noting that only a small amount of DOX (15.4% after 48 h) can be released at pH 7.4 and temperature 37°C, and the linkages/bonds between DOX and carriers will be weakened at increased temperatures and reduced pH values.[23] Evidently, when reducing the pH values from 7.4 to 5.0 and keeping the temperature at 37°C, the DOX release percentage increased from 15.4% to 46.6% after 48 h, and when the temperature changed from 37°C to 43°C and the pH was kept at 5.0, the maximum release amount of DOX showed further increase to 61.1%, much higher than that at 37°C and pH 5.0, which is greatly beneficial to minimize the side effects of chemotherapeutics and enhance the antitumor efficiency. The drug release accelerated with elevating the temperature, which could also be adjusted by the heat from the radiated HPB nanospheres. As seen in Figure 4D, the NIR laser was triggered at predetermined time intervals (0, 60, 120 min), a burst release of DOX can be observed after every laser ON point. The results confirmed that the photothermal effect of HPB nanospheres could also be used in the controlled drug release under NIR laser irradiation.

In vitro Cell Assay

The cell toxicity of HPB nanospheres was firstly evaluated by the MTT assay on HeLa cells, as shown in Figure 5A. With content ranging from 10 to 200 μg mL^{-1}, no significant cytotoxicity of HPB nanospheres was observed for HeLa cells, even at a relatively high concentration of 200 μg mL^{-1}, which proves that HPB nanospheres have good in vitro biosafety. To further investigate the uptake and distribution of HPB-DOX in HeLa cells, the fluorescent cell morphology was characterized to observe CLSM. Obviously, with the assistance of a drug carrier, a large amount of DOX could be transported into HeLa cells easily (Figure 5B). The results indicated that the endocytosed nanoparticles were mostly localized at the cytoplasm as seen from the red color where the DOX molecules were released. The chemotherapy of HPB nanospheres as a drug carrier was then investigated in Figure 5C. At the beginning,

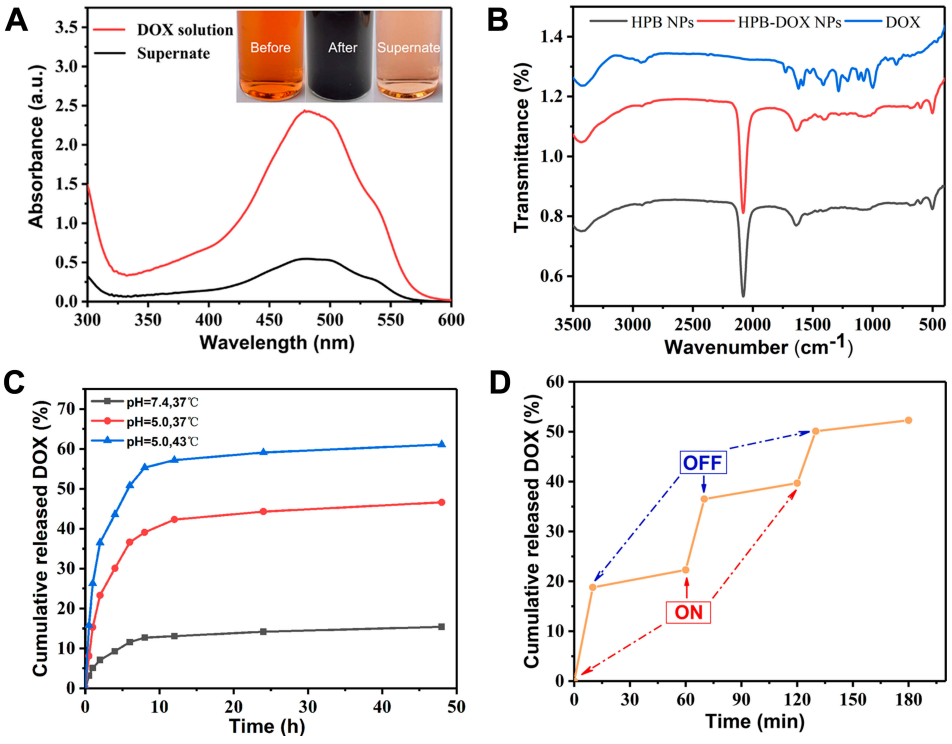

Figure 4 (**A**) UV-Vis-NIR curves of initial DOX solution and the supernatant after loading, (**B**) IR spectra of HPB nanospheres, HPB-DOX nanospheres and DOX, (**C**) release profiles of DOX-loaded HPB nanospheres measured in PBS (pH = 7.4, 5.0) at 37°C and 43°C respectively, (**D**) release profile of DOX-loaded HPB nanospheres measured in PBS (pH = 5.0) at 37°C under NIR laser (808 nm, 1 W cm^{-2}) irradiation for 10 min with an ON/OFF-mode every 60 minutes.

HeLa cells were incubated in 96-well plates at 37°C for 24 h, and then different concentrations of DOX-HPB nanospheres (0, 10, 25, 50, 100 g mL^{-1}) were added, and the mixture was incubated for 24 h. The HeLa cells could be killed with increasing HPB nanospheres, the relative survival proportion decreases from ~100% to 68.8% with the concentration of HPB nanospheres increasing from 0 to 100 μg mL^{-1}.

The photothermal performance of HPB nanospheres was then investigated through ablating tumor cells under laser irradiation in Figure 5D. Similar to the above chemotherapy, HeLa cells were incubated in 96-well plates at 37°C for 24 h, and then different concentrations of HPB nanospheres were added, and the mixture was cultured for 4 h, and then treated with or without 808 nm laser (5 min, 1 W cm^{-2}), respectively. As illustrated in Figure 5D, the cells show high viability in the absence of light; however, the relative survival proportion decreases significantly from ~100% to less than 20% with the concentration of HPB nanospheres increasing from 0 to 100 μg mL^{-1}. Thus, the HPB nanospheres with good biocompatibility could effectively ablate cancer cells under NIR laser.

Although both hyperthermia and chemotherapy can kill tumor cells as shown in Figure 5C and D, the efficiencies were low at a low concentration of 50 μg mL^{-1}. In view of the above results that the laser irradiation could promote the release of DOX loaded in HPB nanospheres, photothermal therapy and chemotherapy were combined to kill the cancer cells. As shown in Figure 5E, the HeLa cells cultured with different active species including PBS, HPB nanospheres, only NIR irradiation, HPB-DOX, free DOX, and HPB-DOX combined with laser irradiation (808 nm laser for 5 min at

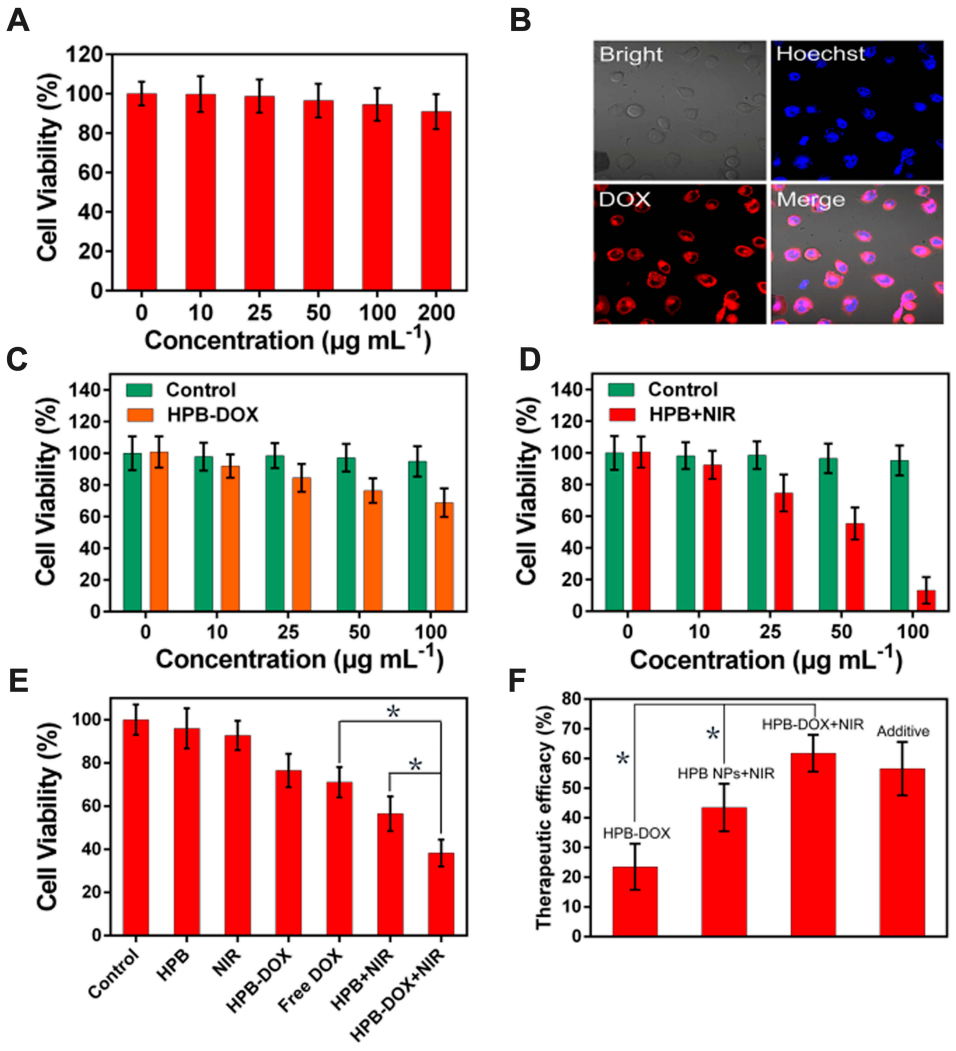

Figure 5 (**A**) The cell toxicity of HPB nanospheres, (**B**) the uptake and distribution of HPB-DOX in HeLa cells, (**C**) cell viability of HeLa cells treated HPB nanospheres with and without HPB-DOX nanospheres at different concentrations and (**D**) cell viability of HeLa cells incubated of HPB nanospheres with and without laser irradiation at different concentrations, (**E**) cell viability of HeLa cells after being incubated in PBS solution containing different active species (mean ± s. e. m., n = 3, *P < 0.05), (**F**) therapeutic efficacy of chemotherapy, photothermal therapy, photothermal/chemo-therapy, and additive therapeutic efficacy (mean ± sem, n = 3, *P < 0.05).

a power density of 1 W cm^{-2}) were investigated for comparison, and then an MTT assay was performed to measure relative cell viability. The free DOX group (28.9%) has relatively higher toxicity than the HPB-DOX group (23.6%), which is due to the limited DOX release from HPB nanospheres. The HPB nanospheres with NIR laser irradiation group results in 43.5% cell mortality rate; however, the HPB nanospheres-DOX+NIR group leads to 61.8% cells being killed. The nominal efficiency of additive therapeutic therapy with the combination of chemo and thermal therapy can be calculated according to the previous report.[27] As shown in Figure 5F, the therapeutic efficacies of single chemotherapy and photothermal therapy are 23.6% and 43.3%, respectively. The calculated additive value of additive is 56.8%, which is lower than that of the HPB nanospheres-DOX+NIR group (61.8%). The relative higher therapeutic efficacy in the real test may be due to the synergistic effect of chemo-thermal therapy. The control results implied that the heat produced by PB shell under the exposure of an NIR laser can promote the ablation of cancer cells with synergistic photothermal/chemo-therapy.

In vivo Antitumor Therapy

The HPB nanospheres exhibited good biocompatibility and treating efficiency in the above in vitro assay. Here the in vivo antitumor experiments were further carried out to evaluate their therapeutic efficacy of tumor. First, the in vivo photothermal effect of HPB nanospheres was measured. The mice bearing HeLa tumors were intratumorally injected with PBS, HPB, DOX-HPB, then subjected to 808 nm laser exposure (1 W cm^{-2}, 5 min). The temperature changes were monitored with an infrared thermal imaging camera in Figure 6A. The nude mice injected with the HPB group and DOX-HPB group presented marked heat production at the tumor site with the temperature of tumor rapidly increasing from 36.2°C to 61.5°C, whereas the surrounding tissue near the tumor only exhibited near-physiological temperature. In contrast, the temperature of mice injected with PBS showed a moderate temperature of about 39°C. The temperature change can be seen clearly from the time–temperature curve in Figure 6B, indicating the excellent photothermal performance of HPB nanospheres under the exposure of NIR laser. Secondly, the photothermal/chemo-synergistic therapeutic efficacy was further evaluated in in vivo tumor treatment. The antitumor efficacy of various treatment groups is illustrated in Figure 6C and D. From the control experiments, the obvious changes could be visually confirmed by comparing the tumors after different treatments in various time durations as shown in the representative digital photos (Figure 6C), and it could be found that the relative tumor volume had significantly decreased after intratumoral injection of DOX-HPB and laser irradiation in Figure 6D. More interestingly, the tumor completely disappeared after 14 days post-treatment. In addition, the

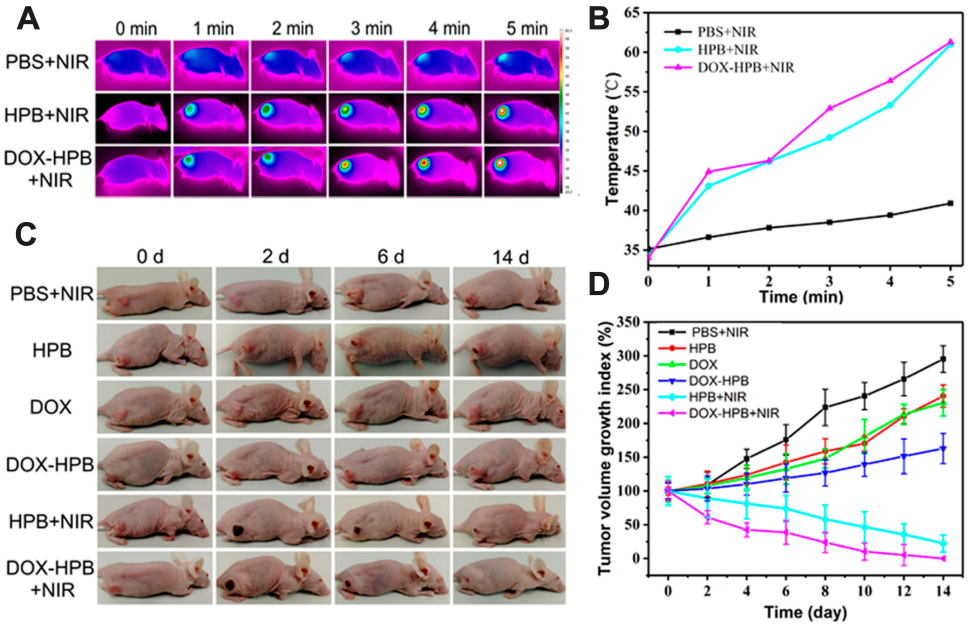

Figure 6 (**A**) Infrared thermal images of control and treatment groups, (**B**) heating curve at different time points of control and treatment groups, (**C**) photographs of mice bearing HeLa tumor after different treatments for varied time periods, (**D**) the relative tumor growth rate with different treatments.

bodyweight of the nude mice in the control group and other treatment groups did not have obvious changes except for the DOX group during the treatment (Figure S8), demonstrating satisfactory in vivo biocompatibility and biosafety of HPB nanospheres. The in vivo experiments confirmed the outstanding performance of HPB nanospheres in photothermal/chemo-synergistic therapy of cancer.

Conclusion

Hollow Prussian blue (HPB) nanospheres were synthesized through the solvent-mediated template route, where the Fe_2O_3 colloidal template played the role of Fe^{3+} source. Under optimal conditions, HPB nanospheres with different shell thicknesses and void sizes were further synthesized based on the designed route. When using HPB nanospheres as a therapeutic agent, they demonstrated a high DOX loading capacity of 440 mg g^{-1} as a drug carrier; meanwhile, the release rate of the loaded DOX in HPB nanospheres could be controlled under the exposure of an NIR laser. Importantly, the in vitro and in vivo results demonstrate that the combination of photothermal/chemo-therapy exhibits low toxicity and high efficiency for cancer therapy. Therefore, the as-synthesized HPB nanospheres are considered as a promising candidate for future cancer therapy due to their excellent integration of NIR photothermal therapy and chemotherapy.

Acknowledgments

This work was supported by the Natural Science Foundation of China (No. 51102077, No. 51372070), the Program for Science & Technology Innovation Talents in Universities of Henan Province (No. 16HASTIT009), the Natural Science Foundation of Henan University (No. 0000A40409), and the key scientific and technological projects in Henan Province (No. 202102310598).

Disclosure

Yongqiang Wang and Long Lu report a patent Monodisperse hollow Prussian blue nanosphere, preparation method, and application pending to CN201910671153.1. The authors report no other possible conflicts of interest in this work.

References

1. Song G, Cheng L, Chao Y, Yang K, Liu Z. Emerging nanotechnology and advanced materials for cancer radiation therapy. *Adv Mater*. 2017;29(32):1700996. doi:10.1002/adma.201700996
2. Peer D, Karp JM, Hong S, Farokhzad OC, Margalit R, Langer R. Nanocarriers as an emerging platform for cancer therapy. *Nat Nanotechnol*. 2007;2(12):751. doi:10.1038/nnano.2007.387
3. Nishiyama N. Nanocarriers shape up for long life. *Nat Nanotechnol*. 2007;2(4):203. doi:10.1038/nnano.2007.88
4. Parhi P, Mohanty C, Sahoo SK. Nanotechnology-based combinational drug delivery: an emerging approach for cancer therapy. *Drug Discov Today*. 2012;17(17–18):1044. doi:10.1016/j.drudis.2012.05.010
5. Yang P, Gai S, Lin J. Functionalized mesoporous silica materials for controlled drug delivery. *Chem Soc Rev*. 2012;41(9):3679. doi:10.1039/c2cs15308d
6. Rosenblum D, Joshi N, Tao W, Karp JM, Peer D. Progress and challenges towards targeted delivery of cancer therapeutics. *Nat Commun*. 2018;9(1):1410. doi:10.1038/s41467-018-03705-y
7. Chen H, Zhang W, Zhu G, Xie J, Chen X. Rethinking cancer nanotheranostics. *Nat Rev Mater*. 2017;2(7):17024. doi:10.1038/natrevmats.2017.24
8. de Melo-diogo D, Pais-Silva C, Dias DR, Moreira AF, Correia IJ. Strategies to improve cancer photothermal therapy mediated by nanomaterials. *Adv Healthc Mater*. 2017;6(10):1700073. doi:10.1002/adhm.201700073
9. Liu Y, Bhattarai P, Dai Z, Chen X. Photothermal therapy and photoacoustic imaging via nanotheranostics in fighting cancer. *Chem Soc Rev*. 2019;48:2053.
10. Chen Y, Wu Y, Sun B, Liu S, Liu H. Two-dimensional nanomaterials for cancer nanotheranostics. *Small*. 2017;13(10):1603446. doi:10.1002/smll.201603446
11. Cheng L, Wang C, Feng L, Yang K, Liu Z. Functional nanomaterials for phototherapies of cancer. *Chem Rev*. 2014;114:10869.
12. Wang J, Li N. Functional hollow nanostructures for imaging and phototherapy of tumors. *J Mater Chem B*. 2017;5:8430.
13. Zhuang H, Su H, Bi X, et al. Polydopamine nanocapsule: a theranostic agent for photoacoustic imaging and chemo-photothermal synergistic therapy. *ACS Biomater Sci Eng*. 2017;3(8):1799.
14. Han L, Hao Y, Wei X, Chen X, Shu Y, Wang J. Hollow copper sulfide nanosphere–doxorubicin/graphene oxide core–shell nanocomposite for photothermo-chemotherapy. *ACS Biomater Sci Eng*. 2017;3:3230.
15. Zhao Q, Yang Y, Wang H, Lei W, Liu Y, Wang S. Gold nanoparticles modified hollow carbon system for dual-responsive release and chemo-photothermal synergistic therapy of tumor. *J Colloid Interf Sci*. 2019;554:239.
16. Fu G, Liu W, Feng S, Yue X. Prussian blue nanoparticles operate as a new generation of photothermal ablation agents for cancer therapy. *Chem Commun*. 2012;48:11567.
17. Xue P, Sun L, Li Q, et al. PEGylated magnetic Prussian blue nanoparticles as a multifunctional therapeutic agent for combined targeted photothermal ablation and pH-triggered chemotherapy of tumour cells. *J Colloid Interf Sci*. 2018;509:384.
18. Luk BT, Fang RH, Hu CM, et al. Safe and immunocompatible nanocarriers cloaked in RBC membranes for drug delivery to treat solid tumors. *Theranostics*. 2016;6:1004.
19. Zhu W, Liu K, Sun X, et al. Mn2+-doped prussian blue nanocubes for bimodal imaging and photothermal therapy with enhanced performance. *ACS Appl Mater Inter*. 2015;7:11575.
20. Xue P, Cheong KKY, Wu Y, Kang Y. An in-vitro study of enzyme-responsive Prussian blue nanoparticles for combined tumor chemotherapy and photothermal therapy. *Colloid Surf B*. 2015;125:277.
21. Cheng L, Gong H, Zhu W, et al. PEGylated Prussian blue nanocubes as a theranostic agent for simultaneous cancer imaging and photothermal therapy. *Biomaterials*. 2014;35(37):9844. doi:10.1016/j.biomaterials.2014.09.004
22. Guo Y, Fang Q, Xu J, et al. Synthesis of mesoporous yolk-shell magnetic Prussian blue particles for multi-functional nanomedicine. *J Nanosci Nanotechnol*. 2018;18(5):3059. doi:10.1166/jnn.2018.14859
23. Chen W, Zeng K, Liu H, et al. Cell membrane camouflaged hollow Prussian blue nanoparticles for synergistic photothermal-/chemotherapy of cancer. *Adv Funct Mater*. 2017;27(11):1605795. doi:10.1002/adfm.201605795

24. Li J, Zhang F, Hu Z, et al. Drug "Pent-Up" in Hollow magnetic Prussian blue nanoparticles for NIR-induced chemo-photothermal tumor therapy with trimodal imaging. *Adv Healthc Mater*. 2017;6(14):1700005. doi:10.1002/adhm.201700005
25. Jing L, Shao S, Wang Y, Yang Y, Yue X, Dai Z. Hyaluronic acid modified hollow Prussian blue nanoparticles loading 10-hydroxycamptothecin for targeting thermochemotherapy of cancer. *Theranostics*. 2016;6(1):40. doi:10.7150/thno.13250
26. Jia X, Cai X, Chen Y, et al. Perfluoropentane-encapsulated hollow mesoporous Prussian blue nanocubes for activated ultrasound imaging and photothermal therapy of cancer. *ACS Appl Mater Inter*. 2015;7(8):4579. doi:10.1021/am507443p
27. Cai X, Jia X, Gao W, et al. A Versatile nanotheranostic agent for efficient dual-mode imaging guided synergistic chemo-thermal tumor therapy. *Adv Funct Mater*. 2015;25(17):2520. doi:10.1002/adfm.201403991
28. Cai X, Gao W, Ma M, et al. A Prussian blue-based core-shell hollow-structured mesoporous nanoparticle as a smart theranostic agent with ultrahigh pH-responsive longitudinal relaxivity. *Adv Mater*. 2015;27(41):6382. doi:10.1002/adma.201503381
29. Lian H, Hu M, Liu C, Yamauchi Y, Wu KCW. Highly biocompatible, hollow coordination polymer nanoparticles as cisplatin carriers for efficient intracellular drug delivery. *Chem Commun*. 2012;48(42):5151. doi:10.1039/c2cc31708g
30. Yang R, Hou M, Gao Y, et al. Indocyanine green-modified hollow mesoporous Prussian blue nanoparticles loading doxorubicin for fluorescence-guided tri-modal combination therapy of cancer. *Nanoscale*. 2019;11(12):5717. doi:10.1039/C8NR10430A
31. Roy X, Hui JKH, Rabnawaz M, Liu G, MacLachlan MJ. Prussian blue nanocontainers: selectively permeable hollow metal–organic capsules from block ionomer emulsion-induced assembly. *J Am Chem Soc*. 2011;133(22):8420. doi:10.1021/ja2016075
32. Liang G, Xu J, Wang X. Synthesis and characterization of organo-metallic coordination polymer nanoshells of Prussian blue using Miniemulsion Periphery Polymerization (MEPP). *J Am Chem Soc*. 2009;131(15):5378. doi:10.1021/ja900516a
33. Hu M, Furukawa S, Ohtani R, et al. Synthesis of Prussian blue nanoparticles with a hollow interior by controlled chemical etching. *Angew Chem Int Edit*. 2012;51(4):984. doi:10.1002/anie.201105190
34. Niu C, Zou B, Wang Y, Chen L, Zheng H, Zhou S. The template-assisted synthesis of polypyrrole hollow microspheres with a double-shelled structure. *Chem Commun*. 2015;51(24):5009. doi:10.1039/C4CC10445E
35. Wang X, Feng J, Bai Y, Zhang Q, Yin Y. Synthesis, properties, and applications of hollow micro-/nanostructures. *Chem Rev*. 2016;116(18):10983. doi:10.1021/acs.chemrev.5b00731
36. Lou XWD, Archer LA, Yang Z. Hollow micro-/nanostructures: synthesis and applications. *Adv Mater*. 2008;20(21):3987. doi:10.1002/adma.200800854
37. Uemura T, Kitagawa S. Prussian blue nanoparticles protected by poly(vinylpyrrolidone). *J Am Chem Soc*. 2003;125(26):7814. doi:10.1021/ja0356582
38. Zhang X, Gong S, Zhang Y, Yang T, Wang C, Gu N. Prussian blue modified iron oxide magnetic nanoparticles and their high peroxidase-like activity. *J Mater Chem*. 2017;6(24):5110. doi:10.1039/c0jm00174k
39. Park SS, Ha C. Hollow mesoporous functional hybrid materials: fascinating platforms for advanced applications. *Adv Funct Mater*. 2012;48(27):1703814. doi:10.1002/adfm.201703814
40. Zou B, Liu Y, Wang Y. Facile synthesis of highly water-dispersible and monodispersed Fe3O4 hollow microspheres and their application in water treatment. *RSC Adv*. 2013;3(45):23327. doi:10.1039/c3ra42716a